

Thermal Effects on Light Emission in Yb³⁺-Sensitized Rare-Earth Doped Optical Glasses

E. A. Gouveia, M. T. de Araujo, and A. S. Gouveia-Neto

Departamento de Física, Universidade Federal de Alagoas

Maceió, 57072-970, AL, Brasil

Received on 31 May, 2000

The temperature effect upon infrared-to-visible frequency upconversion fluorescence emission in off-resonance infrared excited Yb³⁺-sensitized rare-earth doped optical glasses is theoretically and experimentally investigated. We have examined samples of Er³⁺/Yb³⁺-codoped Ga₂S₃:La₂O₃ chalcogenide glasses and germanosilicate optical fibers, and Ga₂O₃:La₂O₃ chalcogenide and fluoroindate glasses codoped with Pr³⁺/Yb³⁺, excited off-resonance at 1.064 μm. The experimental results revealed thermal induced enhancement in the visible upconversion emission intensity as the samples temperatures were increased within the range of 20°C to 260°C. The fluorescence emission enhancement is attributed to the temperature dependent multiphonon-assisted anti-Stokes excitation process of the ytterbium-sensitizer. A theoretical approach that takes into account a sensitizer temperature dependent effective absorption cross-section, which depends upon the phonon occupation number in the host matrices, has proven to agree very well with the experimental data. As beneficial applications of the thermal enhancement, a temperature tunable amplifier and a fiber laser with improved power performance are presented.

I Introduction

The most remarkable feature that called attention to the rare-earth(RE) ions in crystals was the observed sharpness of the many absorption and emission spectral lines [1] and references therein. In many cases these lines can be as narrow as the ones commonly obtained from spectra of free atoms or molecules [1]. This feature is associated with the fact that, as their electronic configuration is 4f^N5s²5p⁶ either for divalent or trivalent ion, the optical active electrons are in the 4f shell such that they are not the outermost ones. They are shielded from external fields by two electronic shells with larger radial extension(5s²5p⁶), which explains the atomiclike behavior of their spectra. As a result, the 4f electrons are weakly perturbed by the static crystal field of the surrounding medium and their energy-levels can be described to a good degree of accuracy with a one-level model. Furthermore, the RE ions in solids have drawn much attention owing to their very impressive characteristic of being very good light emitters in the spectral region covering visible, near-infrared and infrared up to 3.0 μm.

Much effort has recently been focused on the conversion of infrared (IR) radiation into visible light through frequency upconversion in rare-earth doped glassy materials [2], for a wide variety of applications including color displays, high density optical data reading and storage, biomedical diagnostics, infrared laser view-

ers and indicators, amongst many. The frequency upconversion process involves either sequential or multiphoton stepwise excitation and energy transfer between rare-earth ions in solids and subsequent emission of photons with energies higher than the excitation photons [2]. However, for the majority of rare-earth single-doped systems the infrared-to-visible upconversion process has proven inefficient particularly for pumping in the wavelength region of 1.0 μm to 1.1 μm, where high power sources are commercially available. The realization of Yb³⁺-sensitized materials which exploits the high absorption cross-section (peaked around 980 nm) of ytterbium, as compared to other rare-earth ions and the efficient energy-transfer [2,3] mechanism between pairs or triads of rare-earth ions, has allowed a substantial improvement in the upconversion efficiency in ytterbium sensitized Tm³⁺ [4], Er³⁺ [5-7], and Pr³⁺ [8-11] doped bulk glasses and optical fibers. This approach makes it possible the realization of upconversion based photonic devices excited by commercially available high power sources around 1.0 μm. In ytterbium-sensitized rare-earth doped materials, under infrared nonresonant excitation, with the pump-photon energy lower than the 2F_{7/2} → 2F_{5/2} transition of the Yb³⁺ ion, the population of the active ions (acceptors) visible emitting levels is accomplished via an indirect pumping process with multiphonon-assisted anti-Stokes excitation of the sensitizer [12], followed by energy-transfer to the acceptor in the ground-state and a subsequent

absorption from (or energy-transfer to) process to the excited-state. The excited-state absorption can be either resonant or multiphonon-assisted as in the case herein reported. Therefore, the effective pumping of the active ions emitting levels is strongly dependent upon the phonon population in the host material. In this work, thermally induced visible upconversion emission enhancement in ytterbium-sensitized rare-earth doped optical glasses nonresonantly excited at $1.064 \mu\text{m}$ is experimentally and theoretically studied, and application in optical amplifiers and fiber lasers are presented.

II Experimental

The experiment was carried out using $\text{Er}^{3+}/\text{Yb}^{3+}$ -codoped samples of $70\%\text{Ga}_2\text{S}_3:30\%\text{La}_2\text{O}_3$ (Ga:La:S:O) chalcogenide bulk glasses[13-14] with concentrations of 1000 ppm/wt of erbium and different concentrations [5000, 8000, and 10000 ppm/wt] of ytterbium ions, and a 2.0 m length of germanosilicate optical fiber with a concentration of 8000 ppm/wt of ytterbium and 500 ppm/wt of erbium ions. The fiber had a cut-off wavelength around $1.3 \mu\text{m}$. For the $\text{Pr}^{3+}/\text{Yb}^{3+}$ -codoped system, the experimental investigation was conducted using fluorindate glass samples with % molar composition of $(33.5-x)\text{InF}_3-20\text{ZnF}_2-20\text{SrF}_2-16\text{BaF}_2-6\text{GaF}_3-2\text{NaF}-0.5\text{PrF}_3-x\text{YbF}_3$. Fluorindate glasses [15] have recently been the subject of much interest owing to their potential application in photonic devices based on rare-earth doped materials [11,16]. The material presents very good optical quality, is stable against atmospheric moisture, it exhibits low optical attenuation from 250 nm to $8 \mu\text{m}$, and due to the low maximum phonon-energy of $\sim 510 \text{ cm}^{-1}$ [16], it is expected to present significantly lower nonradiative decay rates as compared to fluorozirconate glasses ($\sim 590 \text{ cm}^{-1}$). The inclusion of GdF_3 and NaF in the glass composition has considerably reduced the devitrification process and improved the thermal stability, permitting the realization of fluorindate fibers [17]. The samples had concentration of 5000 ppm/wt of praseodymium and different concentrations of ytterbium ions (5000(I), 10000(II), 15000(III) and 20000(IV) ppm/wt). The excitation source was a cw Nd:YAG laser operated at $1.064 \mu\text{m}$. The pump beam was focused down into the samples by a 5 cm focal length lens and the pump beam waist at the samples location was $\sim 60 \mu\text{m}$. The detection system consisted of a scanning spectrograph with operating resolution of 0.5 nm equipped with a S-20 uncooled photomultiplier tube coupled to a lock-in amplifier and a computer. The temperature of each sample was increased from 20°C up to a maximum of 260°C by placing it into an aluminum oven heated by resistive wire elements. A copper-constantan thermocouple (reference at 0°C) attached to one of the sample's faces was used to monitor the temperature within $\sim 2^\circ\text{C}$ accuracy. For the fiber

sample a pair of x20 uncoated microscope objectives was used to couple the pump light into it and collect the radiation emitted out from the test fiber. The fiber span temperature was increased from 17°C to 180°C using a similar method with the thermocouple attached to the fiber cladding by stripping off the plastic jacket.

III Results and Discussion

In this section we describe both theoretically and experimentally, the thermal enhancement process in two different systems: $\text{Er}^{3+}/\text{Yb}^{3+}$ - and $\text{Pr}^{3+}/\text{Yb}^{3+}$ -codoped glasses.

A. $\text{Er}^{3+}/\text{Yb}^{3+}$ -codoped systems

Fig. 1 shows typical visible upconversion fluorescence spectra of radiation emanating from the Ga:La:S:O sample, at different temperatures for a fixed excitation power of 400 mW. The spectra exhibit three distinct emission bands centered around 530, 555, and 670 nm corresponding to the $^2\text{H}_{11/2}$, $^4\text{S}_{3/2}$, and $^4\text{F}_{9/2}$ transitions to the $^4\text{I}_{15/2}$ ground-state of erbium ions. The spectra clearly illustrate the enhancement of the IR-to-visible upconversion efficiency as the sample was heated from room temperature to 155°C . The typical visible power spectra of radiation exiting the test fiber for a fixed pump power of 700 mW coupled into it, at two different temperatures is illustrated in Fig. 2. The spectral content also exhibits three distinct bands peaked around 530, 550, and 670 nm, corresponding to the $^2\text{H}_{11/2}$, $^4\text{S}_{3/2}$, and $^4\text{F}_{9/2}$ transitions to the $^4\text{I}_{15/2}$ ground-state, respectively and the less intense band around 563 nm is associated with the $^2\text{H}_{9/2} - ^4\text{I}_{13/2}$ transition. The spectra depicted in Fig. 2 also clearly illustrate the enhancement of the infrared-to-visible upconversion efficiency as the fiber temperature was raised, at a fixed excitation power of 700 mW at $1.064 \mu\text{m}$. The upconversion excitation mechanism responsible for the population of the visible and near-infrared emitting levels in $\text{Er}^{3+}/\text{Yb}^{3+}$ -codoped samples excited at $1.064 \mu\text{m}$ has recently been reported for silica-based optical fibers [5] and bulk glasses [6,7]. Therefore, it suffices to mention here that the upconversion pumping process of the excited-state luminescent levels of the Er^{3+} -acceptor is obtained by means of the phonon-assisted anti-Stokes excitation of the Yb^{3+} -sensitizer or donor from the $^2\text{F}_{7/2}$ ground-state to the $^2\text{F}_{5/2}$ excited-state. The excited Yb^{3+} transfers its energy to an Er^{3+} ion, exciting it to the $^4\text{I}_{11/2}$ level, and a subsequent energy-transfer process promotes the Er^{3+} ions from the $^4\text{I}_{11/2}$ to the upper $^4\text{F}_{7/2}$ excited-state. Multiphonon-assisted nonradiative decays from the $^4\text{F}_{7/2}$ excited-state populate the $^2\text{H}_{11/2}$, $^4\text{S}_{3/2}$, and $^4\text{F}_{9/2}$ emitting levels, as it is portrayed in the simplified energy-level diagram presented in Fig. 3. The energy levels related to the 563 nm band were omitted from the diagram of Fig. 3,

since throughout this work we have focused on the more intense visible bands. The excitation of the Yb^{3+} -donor from the $^2\text{F}_{7/2}$ ground-state to the $^2\text{F}_{5/2}$ excited-state, demands the participation of optical phonons in order to compensate for the energy mismatch of $\sim 800 \text{ cm}^{-1}$ between the incident pump photon at $1.064 \mu\text{m}$ (9398 cm^{-1}) and the energy connecting the $^2\text{F}_{7/2} - ^2\text{F}_{5/2}$ transition of the ytterbium ions which is $\sim 10200 \text{ cm}^{-1}$. In Yb^{3+} -doped bulk glasses and optical fibers, the inhomogeneous broadened zero-phonon absorption line is negligible beyond $1.05 \mu\text{m}$ [18]. As a consequence, the Yb^{3+} effective absorption cross-section depends upon the phonon occupation number in the host matrix, which is an increasing function of the medium temperature.

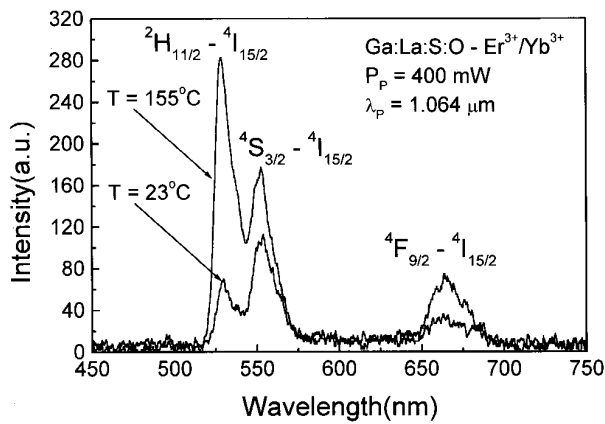


Figure 1. Upconversion emission spectrum at 23 and 155 °C, for a fixed pump power of 400 mW at $1.064 \mu\text{m}$.

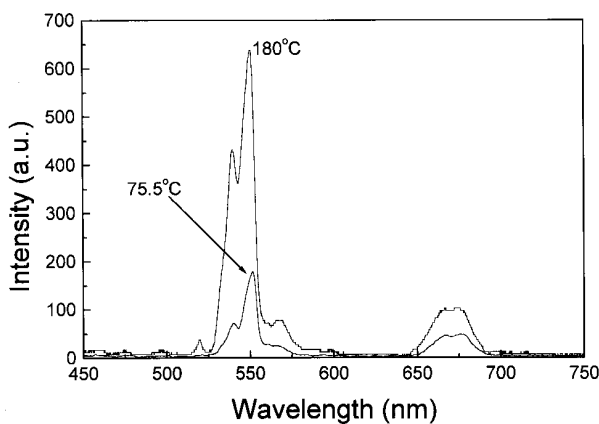


Figure 2. Upconversion power spectra exiting the test fiber at 75.5°C and 180°C , for a fixed pump power of 700 mW at $1.064 \mu\text{m}$.

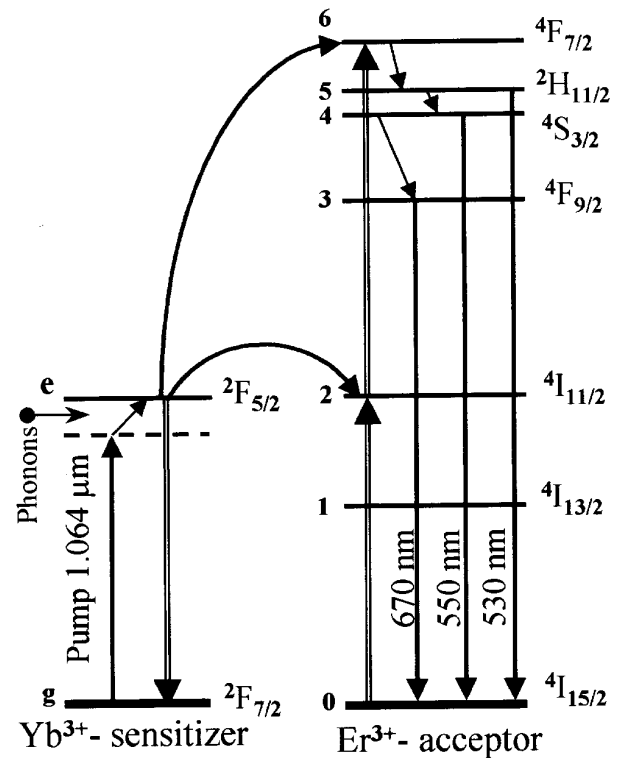


Figure 3. Simplified energy-level diagram of the $\text{Er}^{3+}/\text{Yb}^{3+}$ system. Upward and downwards solid arrows indicate photon absorption and emission, respectively. Double arrows stand for energy-transfer processes and tilted arrows are for multiphonon absorption and emission mechanisms.

The behavior of the visible upconversion emission as a function of sample temperature was investigated and its evolution for the optical fiber case is illustrated in Fig. 4. As can be observed, indeed there exists a steady increase in the visible emission intensities as the fiber was heated from 30°C to 180°C , at a fixed excitation power. A similar behavior was observed for the chalcogenide bulk glass sample. Our observations can be better analyzed, when one examines the visible upconversion fluorescence efficiency as a function of the sample temperature, as indicated in the plots depicted in Figs. 5 and 6. As can be inferred from the experimental data, the integrated visible upconversion fluorescence intensity increased by a factor of three for the Ga:La:S:O glass (Fig. 5) and greater than eight for fiber (Fig. 6) within their range of temperatures.

The experimental results shown in Figs. 5 and 6, are explained using the model portrayed in the energy-level diagram of figure 3, and the set of population rate equations needed to describe the model are listed below as in Ref. 19,

$$\dot{n}_e = n_g \sigma_{ge}(T) \Phi + n_2 C_{2d} n_g - n_e C_{d2} n_0 - \frac{n_e}{\tau_d}, \quad (1.a)$$

$$\dot{n}_6 = n_e C_{d6} n_2 - \frac{n_6}{\tau_6}, \quad (1.b)$$

$$\dot{n}_4 = n_6 W_{64}^{NR} - \frac{n_4}{\tau_4}, \quad (1.c)$$

$$\dot{n}_3 = n_4 W_{43}^{NR} - \frac{n_3}{\tau_3}, \quad (1.d)$$

$$\dot{n}_2 = n_e C_{d2} n_0 - n_2 C_{2d} n_g - \frac{n_2}{\tau_2}, \quad (1.e)$$

where $n_e C_{di} (n_2 C_{2d})$ is the donor (acceptor) energy-transfer rates, which are temperature dependent (see Reference [1-3] and references therein), W_{ij}^{NR} is the nonradiative transition probability, τ_i is the level lifetime, and Φ is the power flux. In Eqs. 1, $\sigma_{ge}(T)$ represents the temperature dependent absorption cross-section for the donor which takes into account the multiphonon-assisted sideband excitation process [12] and it is written as

$$\sigma_{ge}(T) = \sigma_{ge}^0 [\exp(\hbar\omega_{\text{phonon}}/k_B T) - 1]^{-p} \quad (2)$$

In Eq. 2, σ_{ge}^0 is the absorption cross-section at resonance, $\hbar\omega_{\text{phonon}}$ is the phonon energy, k_B is the Boltzmann constant and T is the absolute temperature. The exponent p in Eq. 2 accounts for the number of optical phonons involved in the sensitizer excitation. The steady-state solutions for the set of Eqs. 1(a)-(e) give rise to the population of the thermally coupled ${}^2H_{11/2}$ and ${}^4S_{3/2}$ emitting levels as

$$n_3 = \tau_2 \tau_4 \sigma_{ge}^2(T) N_A N_d^2 C_{d2} C_{d6} \Phi^2 \tau_d^2 \quad (3)$$

In Eq. 3, N_A and N_d are the ion concentration of the acceptor and donor, respectively. In order to get the result in Eq. 3, we have assumed that the direct and back energy transfer between the acceptor and donor do not affect significantly the lifetime of the excited ions, implying that $\tau_d^{-1} \gg n_0 C_{d2}$ and $\tau_2^{-1} \gg n_g C_{2d}$, and for moderate pump intensities the ground-state populations of the $\text{Yb}^{3+} - \text{Er}^{3+}$ pair are not depleted ($n_g \approx N_d$, $n_0 \approx N_A$). Furthermore, the excited-state level ${}^4F_{7/2}$ of Er^{3+} decays simply nonradiatively to ${}^2H_{11/2}$ and ${}^4S_{3/2}$ levels, and multiphonon decay from ${}^2F_{7/2}$ level of Yb^{3+} is not expected due to the large energy separation to the ground-state so that, τ_d is mainly radiative. The observed energy separation between the ${}^2H_{11/2}$ and ${}^4S_{3/2}$ levels was $\Delta E_{45} \approx 700 \text{ cm}^{-1}$, which allows thermal population of the ${}^2H_{11/2}$ level. Correspondingly, the radiative decay time τ_4^R of the ${}^4S_{3/2}$ level is temperature dependent through

$$\frac{1}{\tau_4^R} = \frac{\sum_j A({}^4S_{3/2} \rightarrow j) + 3e^{-\Delta E_{45}/k_B T} \sum_j A({}^2H_{11/2} \rightarrow j)}{1 + 3e^{-\Delta E_{45}/k_B T}}, \quad (4)$$

where $A({}^2H_{11/2}, {}^4S_{3/2} \rightarrow j)$ are radiative transitions rates from the two to the lower lying levels, and the effective populations for the coupled levels are

$$n_4^{eff} = n_4 \frac{1}{1 + 3e^{-\Delta E_{45}/k_B T}} \quad (5a)$$

$$n_5^{eff} = n_4 \frac{3e^{-\Delta E_{45}/k_B T}}{1 + 3e^{-\Delta E_{45}/k_B T}} \quad (5b)$$

Finally, with the proper substitution, the visible emission intensity is obtained through the relation

$$I_{\text{visible}} = \sum_i I_i = \hbar \sum_i \omega_{i0} A_{i0} n_i \quad (6)$$

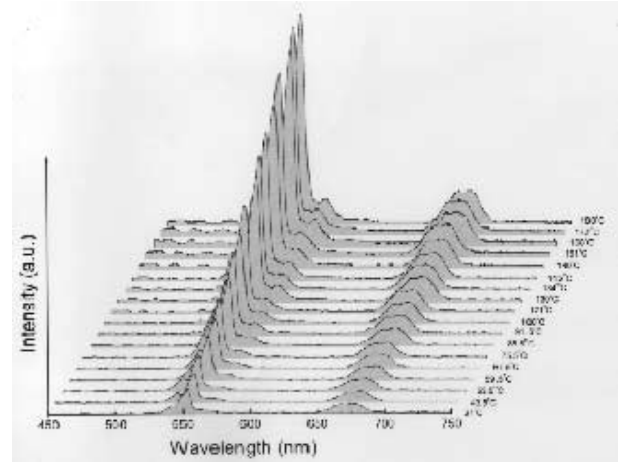


Figure 4. Temperature evolution of the visible upconversion fluorescence emission emanating from the test fiber at a fixed excitation power of 700 mW coupled into it.

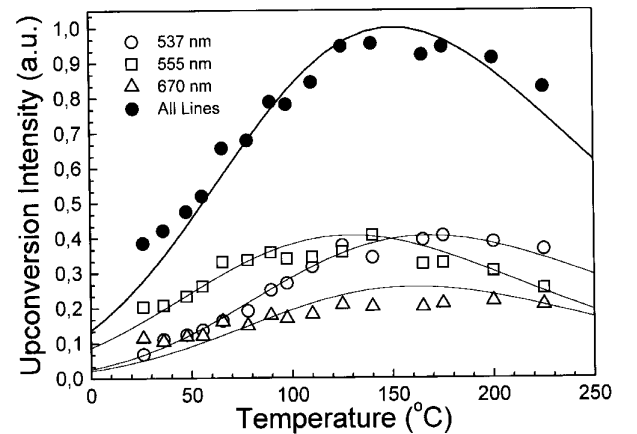


Figure 5. Upconversion emission intensity as a function of temperature for a fixed excitation power of 400 mW. The solid lines represent the theoretical curves obtained from Eqs.5 and 6, adjusted to the experimental data (symbols) for $\text{Ga:La:S:O-Er}^{3+}/\text{Yb}^{3+}$.

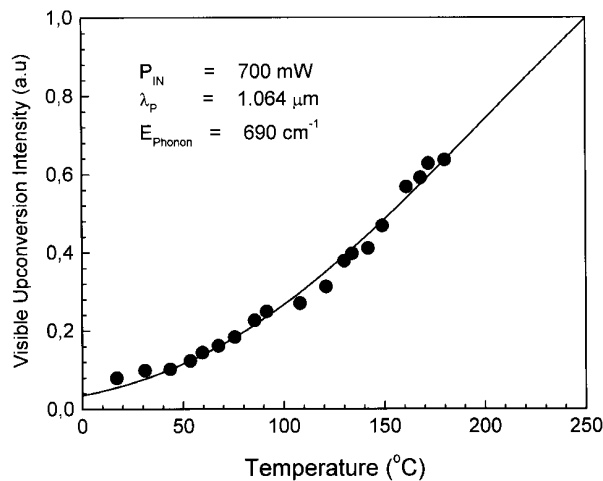


Figure 6. Visible upconversion emission intensity as a function of temperature for a fixed excitation power of 700 mW. The solid line represents the theoretical curve obtained from Eqs. 5 and 6, adjusted to the experimental data (symbols) for $\text{Er}^{3+}/\text{Yb}^{3+}$ -doped fiber.

Based upon these calculations, we need the temperature dependent lifetimes for the participant levels and also the nonradiative transition probabilities. The non-radiative transition probability between levels i and j for low concentration of Er^{3+} ions (our case) is due to multiphonon relaxation processes, and can be related to the temperature by means of the following expression [20]

$$W_{ij}^{NR}(T) = W_{ij}^{NR}(0)[1 - \exp(-\hbar\omega_{\text{phonon}}/k_B T)]^{-p}, \quad (7)$$

where $W_{ij}^{NR}(0)$ is its value at zero temperature. Actually, this probability can be obtained in two ways: subtracting the radiative transition probability (calculated by the Judd-Ofelt theory [21,22]) from the inverse of the observed lifetime or by direct measurement. Furthermore, the energy of the $^4\text{I}_{11/2}$ excited level of Er^{3+} is approximately half of the $^4\text{F}_{7/2}$ level and nearly resonant to the $^2\text{F}_{5/2}$ level of Yb^{3+} , which implies that the temperature dependence of the energy transfer rates C_{di} from Yb^{3+} to Er^{3+} is mainly due to the overlap integrals between the emission of the ytterbium and the absorption of the erbium [23]. However, in several glasses and crystals, the effect of the temperature increase upon the green and red emission of the Er^{3+} , after resonant excitation of the Yb^{3+} -sensitizer, is in the direction of the visible light intensity decrease for the range of temperatures above 20 °C [24]. Hence, the temperature dependence of the upconversion visible light emission associated with the overlap integrals could not account for the temperature behavior exhibited in our findings. The major contribution to the results herein presented is then attributed to the temperature dependence of the ytterbium absorption cross-section as displayed in Eq. (2), and without lack of generality the temperature dependence of the overlap integrals could be neglected in our calculations. Using the calculated radiative transition probabilities and

nonradiative decay rates for chalcogenide [25,26] and silicate glasses [27,28], we have obtained the temperature dependence of the emission intensities of the three visible emission bands as well as of the total visible upconversion emission with the resultant curves indicated by the solid line in plot of Figs. 5 and 6. Indeed, the theoretical model based upon the temperature dependence residing in the effective absorption cross-section of the ytterbium-sensitizer describes quite well our experimental observations for the individual emission intensities at 530, 550, and 670 nm and the integrated visible upconversion emission efficiency. An alternative approach to explain our results would be the possibility that thermal enhancement of the population in the highest lying Stark sublevels of the ytterbium ground-state manifold would give an important contribution to the temperature dependence of the upconversion emission enhancement. However, when one describes the system using only a Boltzmann factor, the theoretical results deviates rapidly from the experimental data for temperatures above 135 °C. The thermal population of the highest Stark sublevels of course produces some enhancement in the upconversion process, but certainly the temperature dependence of the sensitizer absorption cross-section through the multiphonon-assisted anti-Stokes excitation process is the dominant mechanism.

From the results presented in Figs. 5 and 6, we have also obtained the energies of $\sim 345 \text{ cm}^{-1}$ (chalcogenide) and 690 cm^{-1} (optical fiber) for the phonon-modes participating in the multiphonon-assisted anti-Stokes excitation of the sensitizer. This result is to be compared with the ones of 425 cm^{-1} and 1100 cm^{-1} for the maximum phonon-energy associated with $\text{Ga}_2\text{S}_3:\text{La}_2\text{O}_3$ and silica-based glasses, respectively [14, 25-29]. The deviation in the value for the phonon energy obtained in our measurements and the maximum values, is due to the fact that in anti-Stokes sideband excitation processes one has to consider an “effective-phonon-mode”, which has a much lower energy than the host cut-off value [29]. At high temperatures the population distribution of the phonons participating in the excitation process is centered around this low energy “effective-phonon-mode”, as demonstrated both experimentally and theoretically by Auzel and Chen for Er^{3+} -doped ZBLAN and silica glasses [29]. On the other hand, the highest phonon frequency of the host is the one that minimizes the multiphonon order in radiationless emission processes [30,31].

B. $\text{Pr}^{3+}/\text{Yb}^{3+}$ -codoped systems

Much interest has recently been devoted to the search for all-solid-state blue light sources for applications in high-density optical data reading and storage, undersea communications and optical displays. An auspicious approach exploits infrared-to-visible frequency

upconversion in Pr^{3+} -doped materials pumped by commercially obtainable infrared sources. Blue laser operation using frequency upconversion in praseodymium-doped system has already been demonstrated in single- and double-pumped configuration [32-35]. In this section, we demonstrate both experimentally and theoretically that by heating nonresonant infrared excited fluoroindate optical glasses codoped with praseodymium and ytterbium in the temperature region of 20 °C to 260 °C, one obtains up to times twenty blue upconversion emission enhancement. Fig. 7 illustrates the temperature evolution of the visible upconversion emission of light emanating from the sample (IV) at a fixed excitation power of 400 mW at 1.064 μm . It can clearly be seen that the upconversion emission signals increased significantly as the sample's temperature was raised from 20 °C to 260 °C. The spectra depicted in Fig. 7, presented distinct emission bands centered around 485, 530, and 630 nm corresponding to the $^3P_0 \rightarrow ^3H_4$, $^3P_0 \rightarrow ^3H_5$, and $^1D_2 \rightarrow ^3H_4$ transitions of Pr^{3+} ions. Pumping of the Pr^{3+} excited-state visible emitting levels is accomplished through a combination of phonon-assisted absorption, energy-transfer and phonon-assisted excited-state absorption processes, as portrayed in the energy-level diagram depicted in Fig. 8. In a first step, a pump photon at 1.064 μm provokes a multiphonon-assisted anti-Stokes excitation of the Yb^{3+} -sensitizer from the $^2F_{7/2}$ ground-state to the $^2F_{5/2}$ excited-state level. The excited Yb^{3+} transfers its energy to a neighbor Pr^{3+} ion in the 3H_4 ground-state, exciting it to the 1G_4 level. This excited Pr^{3+} ion undergoes a multiphonon-assisted anti-Stokes excited-state absorption of a second pump photon which promotes it to the 3P_0 upper emitting level. Finally, the excited Pr^{3+} ion decays from 3P_0 either radiatively to generate the main visible fluorescence emission bands or nonradiatively to populate lower-lying luminescent levels, as indicated in Fig. 8.

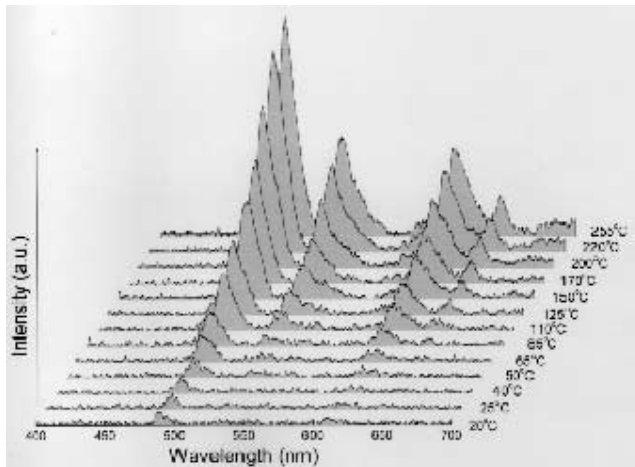


Figure 7. Temperature evolution of the upconversion emission spectrum in $\text{Pr}^{3+}/\text{Yb}^{3+}$ -doped fluoroindate glass. Excitation power of 400 mW at 1.064 μm . Sample IV.

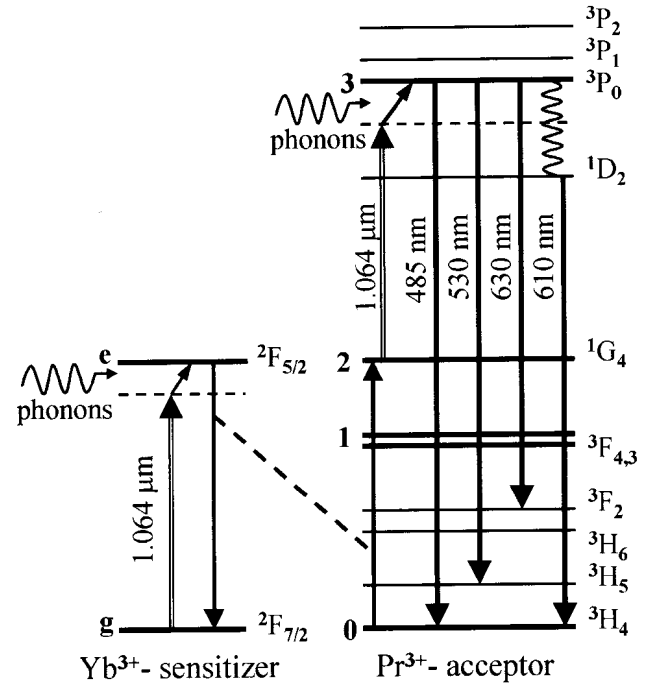


Figure 8. Energy-levels scheme indicating participation of phonons in the absorption transitions. The solid lines connected by a dashed line represents the cross-relaxation process.

The dependence of the blue fluorescence intensity on the excitation power at room temperature and at 115 °C was examined and the results are depicted in the log-log plot of Fig. 9. It was observed that the blue fluorescence exhibited an approximately quadratic power law behavior (slope ~ 2) with pump intensity. Within the excitation power range (up to 1.5 W) of our measurements, the results presented no indication of avalanche processes taking place. The avalanche process is characterized by a nonlinear dependence of the upconversion fluorescence upon the pump power with the existence of a critical power (threshold) [36,37]. However, we have observed the onset of a saturation effect on the emission intensity for pump powers above 700 mW at 115 °C, and 1.0 W at room temperature (20 °C).

The dependence of the blue emission at 485 nm upon temperature was investigated for a fixed pump power of 400 mW, and the results are portrayed in Fig. 10. As can be seen, the 485 nm signal intensity increased by a factor of twenty in the temperature range of 20 °C to 260 °C. The times twenty enhancement in the blue fluorescence intensity was obtained by comparing the integrated spectrum around 485 nm at 260 °C and the one at room temperature (20 °C). The behavior of the $\text{Pr}^{3+}/\text{Yb}^{3+}$ system can be explained as follows. The excitation of the Yb-sensitizer from the $^2F_{7/2}$ ground-state to the $^2F_{5/2}$ excited-state requires the participation of at least two optical phonons in order to compensate for the energy mismatch of $\sim 800 \text{ cm}^{-1}$ between the incident photon and the ytterbium transition energy. Furthermore, the praseodymium $^1G_4 \rightarrow ^3P_0$

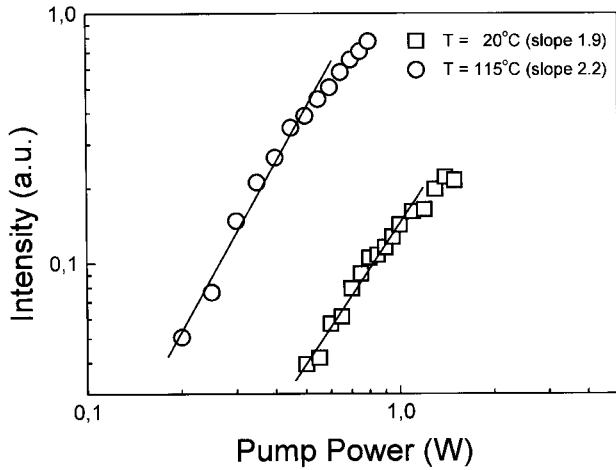


Figure 9. Log-log plot of blue emission intensity as a function of the excitation power in $\text{Pr}^{3+}/\text{Yb}^{3+}$ -doped fluoroindate glass at room temperature (open squares) and at 115 °C (open circles), for sample IV.

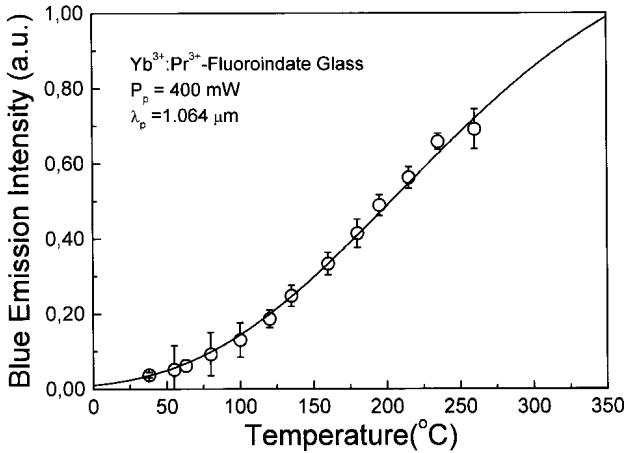


Figure 10. Temperature dependence of the emission signal at 485 nm in $\text{Pr}^{3+}/\text{Yb}^{3+}$ -doped fluoroindate glass. Excitation power of 400 mW at 1.064 μm . Sample IV.

excited-state absorption also demands at least three phonons in order to match the energy difference of approximately 1450 cm^{-1} between the pump-photon energy and that of the Pr^{3+} transition. As a consequence, the population of the Pr^{3+} excited-state $^3\text{P}_0$ level relies strongly on the phonon occupation number in the host matrix. The multiphonon-assisted absorption leads to an effective absorption cross-section for both sensitizer and acceptor, which are increasing functions of the sample temperature giving rise to the enhancement of the emitting levels populations.

The results are analyzed using an approach which includes a phonon-assisted transition in the Yb^{3+} ion ($^2\text{F}_{7/2} \rightarrow ^2\text{F}_{5/2}$), energy-transfer to Pr^{3+} ($^2\text{F}_{5/2} \rightarrow ^1\text{G}_4$), and subsequent phonon-assisted excited-state absorption to populate the $^3\text{P}_0$ level as portrayed in Fig. 8. Accordingly, the temperature dependence of the 485

nm emission intensity is described by the following set of rate-equations:

$$\dot{n}_e = n_g \sigma_{ge}(T) \Phi - n_e C_{S2} n_0 - \frac{n_e}{\tau_S}, \quad (8.a)$$

$$\dot{n}_2 = n_e C_{S2} n_0 - n_2 \sigma_{23}(T) \Phi - \frac{n_2}{\tau_2}, \quad (8.b)$$

$$\dot{n}_3 = n_2 \sigma_{23}(T) \Phi - \frac{n_3}{\tau_3}, \quad (8.c)$$

where $n_e C_{S2}$ is the sensitizer-acceptor energy-transfer rate, τ_S , τ_2 , and τ_3 are the lifetimes of the levels $^2\text{F}_{5/2}$ (level e), $^1\text{G}_4$ (level 2), and $^3\text{P}_0$ (level 3), respectively, and Φ is the power flux. In Eqs. 8, $\sigma_{ge}(T)$ and $\sigma_{23}(T)$ represent the temperature dependent effective absorption cross-sections for the Yb^{3+} excitation and Pr^{3+} excited-state absorption, respectively, which can be written in a general form as given in Eq. 2 [12]. Combining the above equations, one obtains the steady-state population of the blue emitting level as

$$n_3 \cong \frac{\tau_2 \tau_3 \tau_S \sigma_{23}(T) N_A N_S C_{S2} \sigma_{ge}(T) \Phi^2}{(1 + \tau_S \sigma_{ge}(T) \Phi)}, \quad (9)$$

where N_A and N_S are the Pr^{3+} and Yb^{3+} concentrations, respectively. In order to derive Eq. 9, we have assumed $N_S C_{S2} \ll \tau_S^{-1}$ since energy transfer between sensitizer and acceptor must only occur between nearby ions, and also $\sigma_{23} \ll \tau_2^{-1}$ (fulfilled by our experimental conditions), which implies that a small fraction of Pr^{3+} is excited, leading to $n_0 \approx N_A$. The blue light intensity at 485 nm is then given by $I_{485\text{nm}} = h\nu_{30} A_{30} n_3$, where A is the radiative transition rate from level 3 to the ground-state and ν_{30} its frequency.

To obtain the temperature dependence of the blue emission intensity through Eq. 9 we need further considerations to be made. The lifetime of the $^2\text{F}_{5/2}$ level is mainly radiative due to the large energy separation from ground-state (10256 cm^{-1}). The nonradiative transitions from $^1\text{G}_4$ (9696 cm^{-1}) to lower-lying levels are small, as compared to the excited-state pumping rate $^1\text{G}_4 \rightarrow ^3\text{P}_0$ and due to the low maximum-phonon energy associated with fluoroindate hosts [15,16,38], which requires the participation of at least six optical phonons to bridge the energy-gap (3245 cm^{-1}) connecting the levels $^1\text{G}_4 - ^3\text{F}_{3,4}$, resulting in negligible nonradiative transition probability [36]. These mean that the lifetimes τ_s and τ_2 are approximately temperature independent. Moreover, the energy-transfer rate $N_S C_{S2}$ is temperature dependent because of the energy mismatch ($\Delta E_{e2} = 560\text{ cm}^{-1}$) between the $^2\text{F}_{5/2}$ level of Yb^{3+} and the $^1\text{G}_4$ level of Pr^{3+} , and this dependence can be accounted through $\exp(-\Delta E_{e2}/k_B T)$ according to Ref. [12]. Finally, the lifetime of the $^3\text{P}_0$ is related to nonradiative transition probabilities $W_{NR}(T)$ through

$$\tau_3^{-1} = \sum_j A_{3j} + W_{NR}(T), \quad (10)$$

and for low concentrations of rare-earth ions, $W_{NR}(T)$ is due to multiphonon relaxation processes, and given by Eq. 7 [12,20] with an exponent p taking into account the phonon order linking the 3P_0 level (20367 cm^{-1}) to the next lower energy level 1D_2 (16942 cm^{-1}).

Using the experimental lifetime τ_3 for the 3P_0 at room temperature [16] and radiative transitions rate from Ref. [39] for our samples, we have obtained the temperature dependence of the blue emission intensity and the result is illustrated by the solid line in plot of Fig. 10. As can be observed, indeed the theoretical model matches very well the experimental results. A model considering cooperative upconversion of Yb-Yb pairs as the major contribution to the upconversion pumping process of the Pr-acceptor has also been tested but the resultant fitting has fallen far out from the experimental data. The theoretical fitting of data depicted in Fig. 10, also permitted us to withdraw the value of $\sim 400\text{ cm}^{-1}$ for the phonon-mode participating in the multiphonon-assisted anti-Stokes excitation and excited-state absorption of the sensitizer and the acceptor, respectively. The deviation of $\sim 110\text{ cm}^{-1}$ from the value for the maximum phonon-energy associated with fluorindate glasses [38], is attributed to the effect discussed earlier for the $\text{Er}^{3+}/\text{Yb}^{3+}$ -doped system case. We have also performed the same set of experiments using samples I - III, and the results exhibited basically the same behavior as far as blue emission temperature dependence is concerned, as can be inferred from the experimental data depicted in Fig. 11. The upconversion emission efficiencies have followed the same trend with an overall maximum enhancement of approximately x20 for all samples. However, the lower ytterbium concentration samples, required higher pump powers in order to obtain appreciable upconversion fluorescence visible signals.

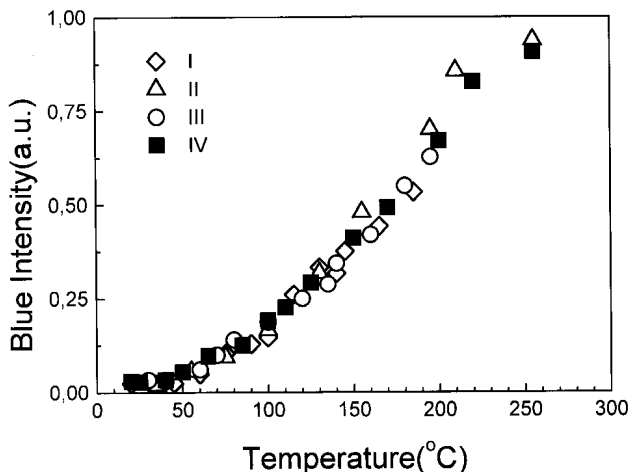


Figure 11. Temperature dependence of the blue emission efficiency for samples I - IV, at fixed pump power in $\text{Pr}^{3+}/\text{Yb}^{3+}$ -doped fluorindate glass.

IV Applications

The effect of temperature on light emission in nonresonant excited ytterbium-sensitized rare-earth doped systems is beneficial in at least two practical situations: upconversion pumped visible light amplification in $\text{Er}^{3+}/\text{Yb}^{3+}$ -codoped chalcogenide glasses and Nd:YAG laser pumped $\text{Er}^{3+}/\text{Yb}^{3+}$ -codoped optical fiber laser at $1.5\ \mu\text{m}$, as we are going to describe next. A. Temperature tunable upconversion pumped amplification. In this section, we describe visible light amplification with temperature enhanced gain in nonresonant $1.064\ \mu\text{m}$ upconversion excited $\text{Er}^{3+}/\text{Yb}^{3+}$ -codoped chalcogenide glasses.

The experiment was carried out in a single-pass signal-pump counterpropagating geometry as depicted in the simplified experimental apparatus of Fig. 12. This configuration prevented the pick up of backwards visible fluorescence owing to the $1.064\ \mu\text{m}$ pump beam. Phase detection also warranted to look at only the signal light. The $\text{Er}^{3+}/\text{Yb}^{3+}$ -codoped chalcogenide glass sample used as amplification medium has already been described in detail in section II. The cw Nd:YAG laser pump beam was focused on the sample by means of a 5 cm focal length lens. The light signals were generated by upconversion fluorescence emission in a Er^{3+} -doped $\text{Ga}_2\text{S}_3:\text{La}_2\text{O}_3$ chalcogenide glass sample pumped at $1.54\ \mu\text{m}$ [40], and were centered around $530, 555,$ and 670 nm corresponding to the maxima of the amplifier gain spectrum. The temperature of the sample was varied in the range of 20°C to 180°C .

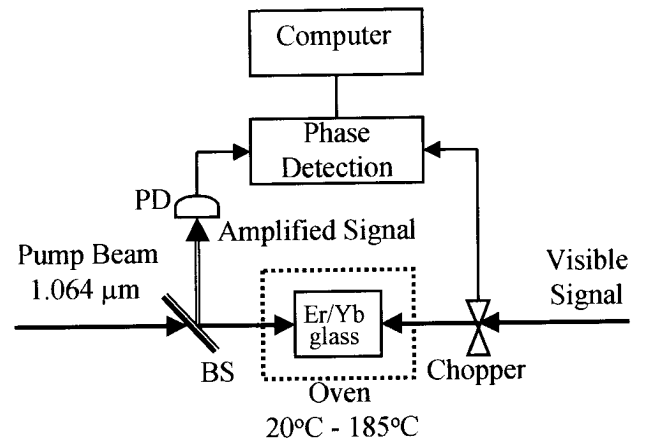


Figure 12. Simplified blok diagram of experimental configuration for the temperature tunable amplifier. In the figure PD is a photodetector and BS is a dichroic beam splitter (100R @ $1.064\ \mu\text{m}$ and highly reflecting in the visible).

The signal amplification on propagation in the gain medium is given by:

$$\partial I_s / \partial z = -\{\alpha_s - \beta_{ps}(T)[Ip]^n\}I_s \quad (11)$$

where z is the propagation distance along the gain medium, $I_{s,p}$ are the light intensities, α_s is the absorption coefficient at the signal wavelength, and indexes s and p stand for signal and pump, respectively. The exponent n determines the number of pump photons involved in the upconversion pumping mechanism. The nonlinear gain coefficient $\beta_{ps}(T)$ is temperature dependent through $\beta_{ps}(T) = \beta_{ps}^0 F(T)$, where β_{ps}^0 is the nonlinear gain coefficient at resonance and $F(T) = [\exp(h\nu_{\text{phonon}}/k_B T) - 1]^{-p}$ as described before. The gain in the amplifier is obtained by upconversion pumping of the $^2H_{11/2}$, $^4S_{3/2}$, and $^4F_{9/2}$, excited-state levels of the Er^{3+} ions, as presented in detail in Ref. [7]. For a fixed glass temperature of 165°C , the signal light intensity as a function of the pump power was evaluated and the results are depicted in Fig. 13. As can clearly be seen the signal has increased by a factor of times six for the highest pump power utilized in our measurements. Furthermore, the experimental results indeed followed the exponential behavior with squared pump power as determined with the integration of Eq. (11) and indicated by the solid line in Fig. 13. In order to integrate Eq. (11) we have assumed the participation of two pump photons ($n = 2$) in the upconversion excitation mechanism of the amplifier medium [7]. It is important to mention that we have also observed a significant reduction in the amplified signal bandwidth as compared to the input signal. The indirect pumping mechanism in the amplification process herein described requires the participation of at least two optical phonons (the maximum phonon-energy associated with Ga:La:S:O glasses is $\sim 425 \text{ cm}^{-1}$ [14]), in order to compensate for the energy-mismatch of $\sim 800 \text{ cm}^{-1}$ between the pump photon-energy and the $^2F_{7/2} - ^2F_{5/2}$ transition of the Yb^{3+} . As a consequence, one has to consider an effective phonon-population dependent nonlinear gain coefficient for the amplifier medium, which in turn is an increasing function of the glass temperature and is determined by $F(T)$. For fixed pump power and input signal intensities, the amplification gain as a function of the amplifier glass temperature was analyzed and results revealed that the optical gain steadily enhanced with increasing temperature as illustrated in plot of Fig. 14. For the temperature range of 20°C to 180°C , the optical gain increased by over 70% when compared to its value at room temperature. Furthermore, it can be inferred from data that the theoretical approach describes quite well the temperature behavior of the amplifier, which is demonstrated by the good agreement between the experimental data and theoretical curve in Fig. 14. The temperature dependence of the amplification process through the effective absorption cross-section of the ytterbium sensitizer shows that one can tune the gain of the Er/Yb amplifier system by varying the glass temperature.

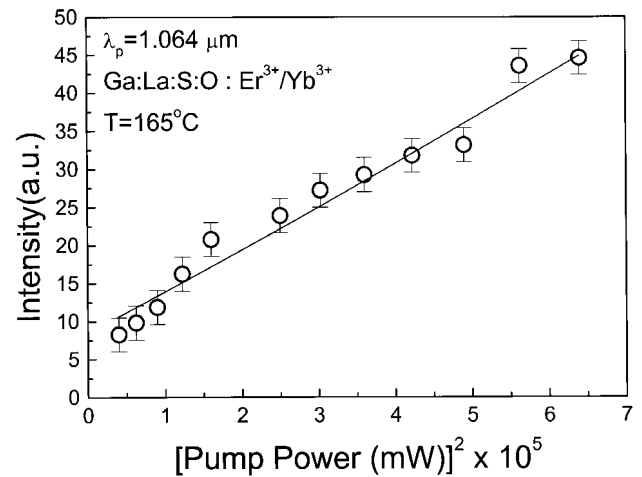


Figure 13. Amplified signal as a function of squared pump power for a fixed temperature of 165°C . Solid line stands for the theoretical fit (Eq. 11) for the experimental data (symbols).

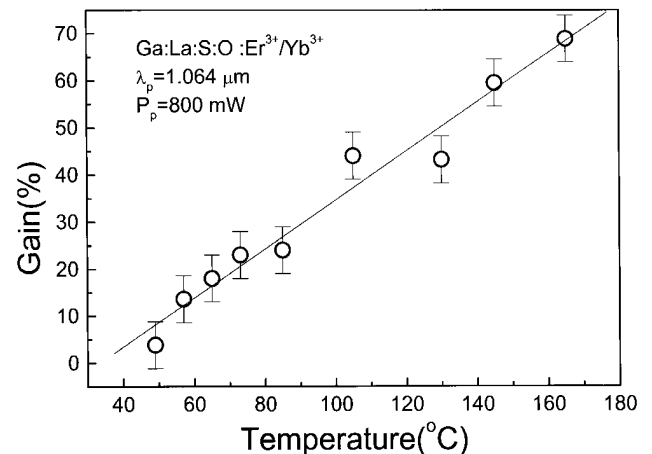


Figure 14. Relative amplification gain as a function of the glass temperature for a fixed pump power of 800 mW at $1.064 \mu\text{m}$.

B. $\text{Er}^{3+}/\text{Yb}^{3+}$ -codoped optical fiber laser pumped at $1.064 \mu\text{m}$

High power Er^{3+} -doped optical fiber sources both narrow and broadband [41-48] operated around $1.5 \mu\text{m}$, are very desirable owing to their potential application in optical communications, sensing, imaging, long range optical time domain reflectometry and telemetry at an eye-safe wavelength. Erbium is a three-level laser medium at $1.5 \mu\text{m}$ so that, it is susceptible to excited-state absorption [49] which is detrimental to the efficiency of the laser. Moreover, erbium singly-doped media offer not only sparse excitation bands in the visible and near infrared, but also possess relatively low absorption cross-sections for the most commonly available pump wavelengths. However, one can overcome these problems by employing Yb^{3+} -sensitized Er^{3+} -doped active media which have been shown to improve substantially the performance and efficiency of optical

amplifiers [50-52], bulk glass lasers [53], and optical fiber and waveguide lasers [54-58]. For several applications is desirable to pursue broadband sources with output powers of a few Watts. Using a cw Nd:YLF laser at $1.054 \mu\text{m}$, a superfluorescent $\text{Er}^{3+}/\text{Yb}^{3+}$ -codoped broadband fiber source generating as much as 1.0 W output power around $1.5 \mu\text{m}$, has recently been demonstrated [59]. For pump wavelengths within this region, the Er^{3+} -ions(acceptor) upper laser level population is accomplished by means of energy-transfer from phonon-assisted anti-Stokes excited Yb^{3+} -ions(sensitizer) [12] and fast nonradiative decay. In this section we present a fourfold output power enhancement and threshold reduction in a $1.064 \mu\text{m}$ pumped $\text{Er}^{3+}/\text{Yb}^{3+}$ -codoped fiber laser by heating the active medium from 23°C to 150°C .

The measurements were conducted using the experimental apparatus illustrated in Fig. 15. The fiber laser consisted of a 2.0 m single-length of $\text{Er}^{3+}/\text{Yb}^{3+}$ -codoped silica based optical fiber forming a spliceless Fabry-Perot oscillator cavity. Feedback was provided by the 3.5% Fresnel reflections at the two glass-air interfaces from the fiber ends. The fiber was doped with 8000 ppm/wt of ytterbium and 500 ppm/wt of erbium and the cut-off wavelength was at 1160 nm. A pair of $\times 10$ uncoated microscope objectives (M.O.) were used to couple the pump light into and collect the radiation emitted out from the fiber sample. A tilted dichroic mirror (100 and 96%T @ $1.54 \mu\text{m}$) was used to block the $1.064 \mu\text{m}$ pump laser light and permitted us to monitor the laser emission in the forward direction. The fiber laser had also a backwards output at the rear-end delivering similar power as in the front end output. The laser active medium temperature was increased from 23°C to 150°C . A typical output emission spectrum from the fiber laser cavity below and above threshold at room temperature is depicted in Fig. 16.

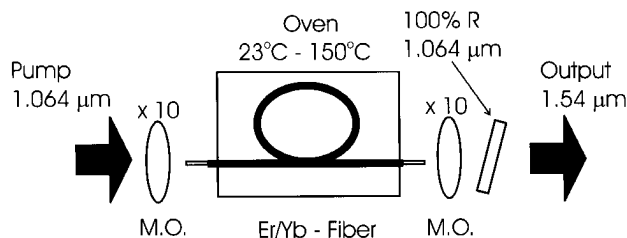


Figure 15. Schematic representation of the experimental apparatus, indicating the $\text{Er}^{3+}/\text{Yb}^{3+}$ -codoped fiber laser in oven.

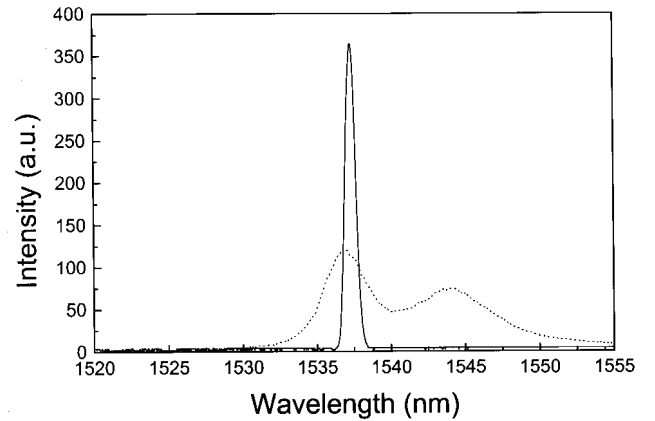


Figure 16. Emission spectrum of the laser below (dotted line) and above (solid line) threshold.

In $\text{Er}^{3+}/\text{Yb}^{3+}$ -codoped laser materials excited off-resonance, by sources with wavelengths in the $1.0 \mu\text{m}$ to $1.1 \mu\text{m}$ range, the population of the erbium upper laser level is achieved indirectly through the phonon-assisted excitation of the Yb^{3+} -sensitizer [12] which efficiently transfers its energy to a neighbor Er^{3+} ion (acceptor) in the ground-state promoting it to the $^4\text{I}_{11/2}$ excited-state level. A fast nonradiative decay from the $^4\text{I}_{11/2}$ populates the $^4\text{I}_{13/2}$ upper laser level, as illustrated in the simplified energy-level diagram of Fig. 17. It is important to point out that the excitation of the ytterbium-sensitizer requires the participation of at least one optical phonon to compensate for the energy mismatch of $\sim 800 \text{ cm}^{-1}$ between the pump photon energy ($\sim 9400 \text{ cm}^{-1}$) and the of the ytterbium $^2\text{F}_{7/2} - ^2\text{F}_{5/2}$ transition ($\sim 10200 \text{ cm}^{-1}$). Consequently, the laser pump-rate depends strongly upon the phonon population in the gain medium. This behavior is accounted for here, by introducing a temperature dependent effective absorption cross-section for the Yb^{3+} -sensitizer as described previously in Eq.(2). For the fiber laser case, we may assume that $p = 1$ since the pump energy mismatch ($\sim 800 \text{ cm}^{-1}$) corresponds approximately to the value of the peak of the phonon spectrum for silicate glasses.

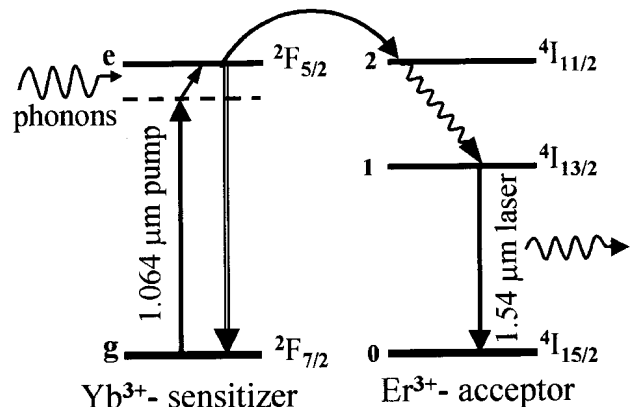


Figure 17. Simplified energy-level diagram for the $\text{Er}^{3+}/\text{Yb}^{3+}$ -doped fiber laser.

By using simple rate-equations and bearing in mind that the laser medium is codoped with ytterbium, we have derived with a fairly accurate approximation the threshold power for the $\text{Er}^{3+}/\text{Yb}^{3+}$ -fiber laser system as $P_{\text{th}} \approx N_E h \nu_p \delta_c A_f / N_Y \sigma_Y(T) \tau_E$ [53,60,61], where N_E and N_Y are the concentrations of erbium and ytterbium ions, respectively, τ_E is the ${}^4\text{I}_{13/2}$ level lifetime, ν_p the pump frequency, and A_f is the fiber effective core area. The parameter δ_c accounts for the cavity losses, pump mode characteristics and output coupling. It is important to point out that in our calculations the direct pumping of erbium was neglected owing to the much lower Er^{3+} concentration as compared to Yb^{3+} . The effective absorption cross-section $\sigma_Y(T) = \sigma_Y^0 [\exp(h\nu_{\text{phonon}}/k_B T) - 1]^{-1}$ is an increasing function of the temperature which in turn leads to a threshold power that steadily decreases as the temperature of the laser medium rises. When laser oscillation commences, the population inversion is locked at the threshold value and the laser output power is directly proportional to the pump-rate (pump power). Bearing that in mind and utilizing a similar analysis as has just been done for the threshold power, one can easily infer that above threshold the fiber laser output power is an increasing function of the active medium temperature via a temperature dependent effective pump power $P_p(T) = P_p^T F(T)$, where P_p^T is the actual 1.064 μm power at a fixed temperature.

In order to verify experimentally our assumptions, the laser threshold power as a function of the fiber temperature was investigated and the results are depicted in Fig. 18. As can be observed from data, indeed the threshold power presented a continuous and smooth decrease with increasing temperature and the experimental results are in reasonable agreement with theory (solid line in graph of Fig. 18). For the temperature range of 36 $^\circ\text{C}$ to 130 $^\circ\text{C}$, a fourfold reduction in the threshold power was achieved. The measurements for the acquisition of each data point were carried out by fixing the fiber temperature and carefully adjusting the pump power in order to just commence laser oscillation. The dependence of the fiber laser output power at 1.54 μm upon temperature for a fixed pump intensity was also analyzed and the results are also depicted in Fig. 18. As can be inferred from data, the output power has increased by a factor of x2.4 when the fiber temperature was varied from 30 $^\circ\text{C}$ to 120 $^\circ\text{C}$. For the highest temperature of 150 $^\circ\text{C}$ used in our measurements, as much as 180 mW output power was generated corresponding to a fourfold output power enhancement as compared to the room-temperature (23 $^\circ\text{C}$) value of 46 mW. It is important to call attention for the good agreement between theoretical (solid line in plot of Fig. 18) and experimental results. We have also evaluated the wavelength stability of the fiber laser system as the temperature increased and the results indicated no detectable change in the emission central wavelength within the

0.5 nm resolution of our system. Moreover, the laser output did not present any distinct intensity fluctuation for high temperatures as compared to the room temperature behavior ($\pm 5\%$).

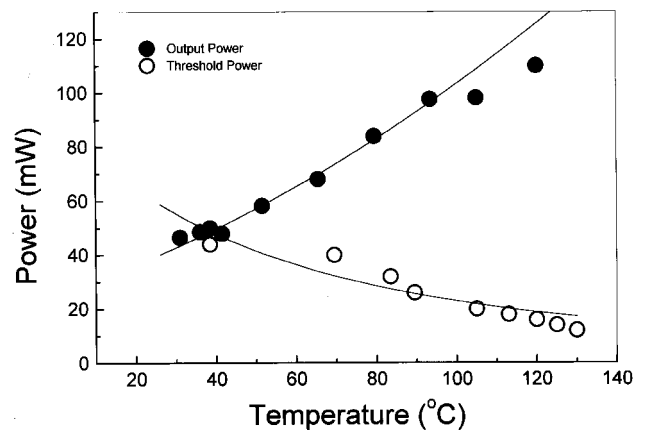


Figure 18. Threshold power and output power for the $\text{Er}^{3+}/\text{Yb}^{3+}$ -doped fiber laser system at 1.54 μm as a function of the fiber temperature. The solid lines stand for the theoretical curves adjusted to the experimental data (symbols).

V Conclusions

In conclusion, the experimental and theoretical investigation of thermally-induced infrared-to-visible upconversion fluorescence emission enhancement in Yb^{3+} -sensitized rare-earth doped optical glasses nonresonant excited at 1.064 μm was examined for different host materials and geometries. For $\text{Er}^{3+}/\text{Yb}^{3+}$ -codoped systems, thermally-induced threefold and eightfold efficiency enhancement for $\text{Ga}_2\text{S}_3:\text{La}_2\text{O}_3$ chalcogenide glasses [62] and germanosilicate optical fiber [63], respectively, was demonstrated. For the $\text{Pr}^{3+}/\text{Yb}^{3+}$ -codoped fluorindate glass sample, our results revealed a twentyfold enhancement in the 485 nm blue emission intensity as the temperature of the glass sample was varied in the 20 $^\circ\text{C}$ - 260 $^\circ\text{C}$ range [64]. The temperature induced visible upconversion emission enhancement for the codoped systems was assigned to the temperature dependent effective absorption cross-section for the ytterbium-sensitizer excitation and acceptor excited-state absorption. Models based upon conventional rate-equations considering the effective absorption cross-sections of both sensitizer and acceptor as functions of the phonon population in the host matrix, agreed very well with experimental data. As beneficial applications of our proposals, we have presented upconversion pumped visible light amplification with temperature tunable gain in $\text{Er}^{3+}/\text{Yb}^{3+}$ -codoped chalcogenide glass [65] and thermally-induced fourfold output power increase and threshold reduction in a $\text{Er}^{3+}/\text{Yb}^{3+}$ -codoped optical fiber laser [66]. In addition,

it can be used to improve the performance, by reducing the inherent thermal noise at high temperatures of optical temperature sensing devices based upon up-conversion fluorescence emission in $\text{Er}^{3+}/\text{Yb}^{3+}$ -codoped glasses and fibers pumped at $1.064 \mu\text{m}$ [67-69].

Acknowledgements

The financial support for this work by FINEP (Financiadora de Estudos e Projetos), CNPq (Conselho Nacional de Desenvolvimento Científico e Tecnológico), CAPES (Coordenadoria de Aperfeiçoamento de Pessoal de Ensino Superior) and PADCT (Programa de Apoio ao Desenvolvimento Científico e Tecnológico), and PRONEX-NEON (UFPE/UFAL/UFPB) is gratefully acknowledged. Our special thanks to all of our collaborators: Prof. Cid B. de Araújo(UFPE), Y. Messaddeq(UNESP), A. S. B. Sombra and J. A. Medeiros Neto(UFCE), that contributed decisively to the realization of this work and to our graduate students P. V. dos Santos, A. S. Oliveira, S. F. Félix, and C. J. da Silva.

References

- [1] S. Hüfner, *Optical spectra of transparent rare earth compounds*, Academic Press, London 1978.
- [2] F. Auzel, *Pro. IEEE* **61**, 758 (1973).
- [3] F. Auzel, *J. Lumin.* **45**, 341 (1990).
- [4] D. C. Hanna, R. M. Percival, I. R. Perry, R. G. Smart, J. E. Townsend, and A. C. Tropper, *Opt. Comm.* **78**, 187 (1990).
- [5] Y-M. Hua, Q. Li, Y-L Chen, and Y-X Chen, *Opt. Comm.* **88**, 441 (1992).
- [6] A. S. Oliveira, M. T. de Araujo, A. S. Gouveia-Neto, A. S. B. Sombra, J. A. Medeiros Neto, and N. Aranha, *J. Appl. Phys.* **83**, 604 (1998).
- [7] A. S. Oliveira, M. T. de Araujo, A. S. Gouveia-Neto, A. S. B. Sombra, J. A. Medeiros Neto, and Y. Messaddeq, *Appl. Phys. Lett.* **72**, 753 (1998).
- [8] D. M. Baney, G. Rankin, and K. W. Chang, *Appl. Phys. Lett.* **69**, 1662 (1996).
- [9] T. R. Gosnell, *Elect. Lett.* **33**, 411 (1997).
- [10] D. M. Baney, G. Rankin, and K. W. Chang, *Opt. Lett.* **21**, 1372 (1996).
- [11] W. Lozano B., C. B. de Araújo, C. E. Egalon, A. S. L. Gomes, B. J. Costa, and Y. Messaddeq, *Opt. Comm.* **153**, 271 (1998).
- [12] F. Auzel, *Phys. Rev.* **B13**, 2809 (1976).
- [13] P. N. Kumta, and S. H. Risbud, *J. Mat. Sci.* **27**, 1135 (1994).
- [14] D. W. Hewak, J. A. Medeiros Neto, B. N. Samson, R. S. Brown, K. P. Jedrzejewski, J. Wang, E. Taylor, R. I. Laming, G. Wylangowski, and D. N. Payne, *IEEE Phot. Techn. Lett.* **6**, 609 (1994).
- [15] Y. Messaddeq, and M. Poulain, *Mater. Scie. Forum*, **67-68**, 161 (1989).
- [16] See for example: W. Lozano B, Cid B. de Araújo, L. H. Acioli, and Y. Messaddeq, *J. Appl. Phys.* **84**, 2263 (1998); E. Martins, Cid B. de Araújo, J. R. Delben, A. S. L. Gomes, B. J. da Costa, and Y. Messaddeq, *Opt. Comm.* **158**, 61 (1998); G. S. Maciel, L. de S. Menezes, Cid B. de Araújo, and Y. Messaddeq, *J. Appl. Phys.* **85**, 6782(1999), and references therein.
- [17] Fibers of fluorindate glass have been developed by Le Verre Flouré (France) since 1998-M. Poulain, (private communications).
- [18] R. Paschotta, J. Nilsson, A. C. Tropper, and D. C. Hanna, *IEEE J. Quant. Elect.* **33**, 1049 (1997).
- [19] J. C. Wright, *Top. Appl. Phys.* **15**, 239 (1976).
- [20] M. J. Weber, *Phys. Rev.* **B8**, 54 (1973).
- [21] B. R. Judd, *Phys. Rev.* **127**, 750 (1962).
- [22] G. S. Ofelt, *J. Chem. Phys.* **37**, 511 (1962).
- [23] T. Miyakawa and D. L. Drexler, *Phys. Rev.* **B1**, 2961 (1970).
- [24] D. C. Yeh, W. A. Sibbey, M. Suscavage, and M. G. Drexhage, *J. Appl. Phys.* **62**, 266 (1987).
- [25] C. C. Ye, D. W. Hewak, M. Hempstead, B. N. Samson, and D. N. Payne, *J. Non-Cryst. Sol.*, **208**, 56 (1996).
- [26] H. Higuchi, M. Takahashi, Y. Kawamoto, K. Kadono, T. Ohtsuki, N. Peyghambarian, and N. Kitamura, *J. Appl. Phys.* **83**, 19 (1998).
- [27] J. A. Capobianco, G. Prevost, P. P. Proulx, P. Kabro, and M. Bettinelli, *Opt. Mat.* **6**, 175 (1996).
- [28] C. B. Layne, W. H. Lowdermilk, and M. J. Weber, *Phys. Rev. B* **16**, 10 (1977).
- [29] F. Auzel, and Y. H. Chen, *J. Lumin.* **66&67**, 224 (1996).
- [30] E. Okamoto, H. Masui, K. Muto, and K. Awazu, *J. Appl. Phys.* **43**, 2122 (1973).
- [31] M. D. Shinn, W. A. Sibbey, M. G. Drexhage, and R. N. Brown, *Phys. Rev. B* **27**, 6635 (1983).
- [32] J. Y. Allain, M. Monerie, and H. Poignant, *Elect. Lett.* **26**, 166 (1990).
- [33] R. G. Smart, D. C. Hanna, A. C. Tropper, S. T. Davey, S. F. Carter, and D. Szebesta, *Elect. Lett.* **27**, 1307 (1994).
- [34] Y. Zhao, and S. Poole, *Elect. Lett.* **30**, 967 (1994).
- [35] Y. Zhao, S. Fleming, and S. Poole, *Opt. Comm.* **114**, 285 (1995).
- [36] J. S. Chivian, W. E. Case, and D. D. Eden, *Appl. Phys. Lett.* **35**, 124 (1974).
- [37] T. R. Gosnell, *Elect. Lett.* **33**, 411 (1997).
- [38] R. M. Almeida, J. C. Pereira, Y. Messaddeq, and M. Aegerter, *J. Non-Cryst. Solids* **161**, 105 (1993).
- [39] A. Flórez, O. L. Malta, Y. Messaddeq, M. A. Aegerter, *J. Non-Cryst. Solids* **213&214**, 315 (1997).
- [40] H. T. Amorim, M. T. de Araujo, E. A. Gouveia, A. S. Gouveia-Neto, J. A. Medeiros Neto, A. S. B. Sombra, *J. Lumin.* **78**, 271 (1998).

- [41] R. J. Mears, L. Reekie, and I. M. Jauncey, Proceedings of CLEO, Optical Society of America, Baltimore, paper WD3, 122 (1987).
- [42] P. Milinski, J. Chrostowsky, A. Koningstein, and J. R. Simpson, IEEE J. Quant. Elect. **28**, 371 (1992).
- [43] P. R. Morkel, K. P. Jedrzejewski, E. R. Taylor, and D. N. Payne, IEEE Phot. Tech. Lett. **4**, 545 (1992).
- [44] A. Chandonnet, and G. Larose, Opt. Eng. **32**, 2031 (1993).
- [45] I. N. Duling III, W. K. Burns, and I. Goldberg, Opt. Lett. **15**, 33 (1990).
- [46] K. Iwatsuki, IEEE Phot. Tech. Lett. **2**, 237 (1990).
- [47] P. F. Wysocki, M. J. F. Digonnet, and B. Y. Kim, Opt. Lett. **16**, 961 (1991).
- [48] P. F. Wysocki, M. J. F. Digonnet, B. Y. Kim, and H. J. Shaw, IEEE J. Lightwave Tech. **12**, 550 (1994).
- [49] R. I. Laming, S. B. Poole, and E. J. Tarbox, Opt. Lett. **13**, 1084 (1988).
- [50] S. G. Grubb, W. F. Humer, R. S. Cannon, T. H. Windhorn, S. W. Vendeta, K. L. Sweeney, P. A. Lailabady, M. R. Keur, J. G. Kwasegroh, T. C. Munks, and D. W. Anthon, Elect. Lett. **28**, 1275 (1992).
- [51] J. D. Minelly, W. L. Barnes, R. I. Laming, P. R. Morkel, J. E. Thownsend, S. G. Grubb, and D. N. Payne, IEEE Phot. Tech. Lett. **5**, 301 (1993).
- [52] Z. J. Chen, J. D. Minelly, and Y. Gu, Elect. Lett. **32**, 1812 (1996).
- [53] P. Laporta, S. de Silvestri, V. Magni, and O. Svelto, Opt. Lett. **16**, 1952 (1991).
- [54] J. T. Kringlebotn, P. R. Morkel, L. Reekie, J. -L. Archambault, and D. N. Payne, IEEE Phot. Tech. Lett. **5**, 1162 (1993).
- [55] J. T. Kringlebotn, J. -L. Archambault, L. Reekie, J. E. Thownsend, G. G. Vienne, and D. N. Payne, Elect. Lett. **30**, 972 (1994).
- [56] F. di Pasquale, and M. Federighi, IEEE Phot. Tech. Lett. **7**, 623 (1995).
- [57] A. Yenyay, J.-M. P. Delavaux, J. Toulouse, D. Barbier, T. A. Strasser, and J. R. Predrazanni, Elect. Lett. **33**, 1792 (1997).
- [58] L. Goldberg, and J. Koplow, Elect. Lett. **34**, 2027 (1998).
- [59] S. Gray, J. D. Minelly, A. B. Grudinin, and J. E. Caplen, Elect. Lett. **33**, 1382 (1997).
- [60] M. J. F. Digonnet, IEEE J. Lightwave Tech. **4**, 1631 (1986).
- [61] E. Tanguy, C. Larat, and J. P. Pohlle, Opt. Commun. **153**, 172 (1998).
- [62] P. V. dos Santos, E. A. Gouveia, M. T. de Araujo, A. S. Gouveia-Neto, A. S. B. Sombra, and J. A. Medeiros Neto, Appl. Phys. Lett. **74**, 3607 (1999).
- [63] C. J. da Silva, M. T. de Araujo, E. A. Gouveia, and A. S. Gouveia-Neto, Appl. Phys. B **70**, 185 (2000).
- [64] A. S. Oliveira, E. A. Gouveia, M. T. de Araujo, A. S. Gouveia-Neto, C. B. de Araújo, and Y. Messaddeq, J. Appl. Phys. **87**, 4274 (2000).
- [65] S. F. Felix, E. A. Gouveia, M. T. de Araujo, A. S. B. Sombra, and A. S. Gouveia-Neto, J. of Lumin. **87-89**, 1020 (2000).
- [66] C. J. da Silva, M. T. de Araujo, E. A. Gouveia, and A. S. Gouveia-Neto, Opt. Lett. **24**, 1287 (1999).
- [67] H. Berthou, and C. K. Jorgensen, Opt. Lett. **15**, 1100 (1990).
- [68] P. V. dos Santos, M. T. de Araujo, A. S. Gouveia-Neto, J. A. Medeiros Neto, and A. S. B. Sombra, Appl. Phys. Lett. **73**, 578 (1998).
- [69] P. V. dos Santos, M. T. de Araujo, A. S. Gouveia-Neto, J. A. Medeiros Neto, and A. S. B. Sombra, IEEE J. Quant. Elect. **35**, 395 (1999).